JMEPEG (2012) 21:1728–1736
DOI: 10.1007/s11665-011-0058-2

1059-9495/$19.00

Microstructure and Mechanical Properties of As-Cast Ductile Irons Alloyed with Manganese and Copper

Ranjan Kumar Dasgupta, Dipak Kumar Mondal, Ajit Kumar Chakrabarti, and Ashis Chandra Ganguli

(Submitted October 19, 2010; in revised form June 1, 2011)

The present investigation was carried out to study the effect of manganese and copper addition, singly as well as in combination, on the microstructure, micro-segregation, and mechanical properties of ductile irons. Alloy A (3.18C, 2.64Si, 0.45Mn), alloy B (3.35C, 2.51Si, 0.82Mn), alloy C (3.16C, 2.80Si, 1.08Mn, 0.56Cu), and alloy D (3.18C, 3.00Si, 1.04Mn, 1.13Cu) were melted and cast in the form of Y-block test pieces. The cast microstructures varied from ferrito-pearlitic in alloys A, B, and C to pearlitic in alloy D. However, on XRD analysis and SEM examination, the presence of martensite patches was also detected. There was a marginal decrease in nodule count in alloy B. In alloys C and D, nodule counts were higher, but the proportion of ferrite decreased drastically. Alloy D was found to be the strongest (UTS ≈ 800 MPa, El = 5%) with alloys A and C coming next in strength; while alloy B was weakest of the four. The presence of martensite patches in association with pearlite appears to be responsible for low toughness of these alloys. Microprobe analysis shows some silicon segregation near the graphite nodules and practically little segregation of manganese. Elemental mapping by FE-SEM does not indicate any manganese segregation.

Keywords austenite, critical temperature, ductile iron, ferrite, fractography, hardness, martensite, microstructure, nodule count, pearlite, toughness

1. Introduction

High strength alloyed ductile irons conforming to BS specifications 600/3 or 700/2 are finding applications in engineering components requiring an optimum combination of strength, toughness and machinability, and low cost. In commercial practice, nickel (0.5-1.0%), copper (0.2-0.3%), and molybdenum (0.1-0.2%) are common alloying elements in high strength ductile irons (Ref 1, 2). A cheaper alloying element like manganese can also be added to stabilize pearlite and increase strength; but a high manganese level (>0.3%) is generally avoided, because it tends to suffer segregation in inter-cellular regions. On the contrary, silicon and copper suffer negative segregation (Ref 3, 4). In addition, the pearlite stabilizing and hardening effect of manganese and copper are well documented (Ref 5, 6). In view of the rising trend in the international cost of nickel and molybdenum, there is a renewed interest in exploiting the strengthening effect of manganese and copper in ductile irons as well. Both manganese and copper are fcc metals and are highly soluble in austenite. An exercise was, therefore, initiated to study the effect of manganese additions up to about 1.0%, singly as well as in combination with 0.5-1.0% copper on as-cast microstructure, mechanical properties, and micro-segregation in ductile irons.

Ranjan Kumar Dasgupta, Materials Engineering Division, Central Mechanical Engineering Research Institute, Durgapur, India; and **Dipak Kumar Mondal, Ajit Kumar Chakrabarti,** and **Ashis Chandra Ganguli**, Department of Metallurgical and Materials Engineering, National Institute of Technology, Durgapur, India. Contact e-mail: dk_mondal2003@yahoo.co.in.

2. Experimental Methods

The experimental alloys designated as A, B, C, and D were melted in a 200 kg acid lined induction furnace using steel scrap (C—0.23%, Si—0.11%, Mn—0.46%, S—0.025%, and P—0.05%), ferro-silicon (Si—70%), ferro-manganese (Mn—80%), electrolytic copper(Cu—99.9%), and graphite. The bath was super heated to 1500 °C. The slag formed was thickened by a slag coagulator (Brand: FOSECO SLAX 30) and then removed. Copper was added to the melt in the ladle. Fe-Si-Mg alloy containing Si—40%, Mg—10%, and Ce—1% was added to the melt using plunging technique with the help of a perforated graphite plunger. After magnesium treatment, the melt was post-inoculated with powdered ferro-silicon so as to raise the silicon percent in the melt by 0.5. A covering flux was added to fix up dross. The dross was skimmed off. The melt was then poured into dry sand Y-block molds at around 1400 °C. The dimensions of a Y-block are shown in Fig. 1. Cleaned coupons of Y-blocks were subjected to radiographic test to ascertain the absence of casting defects, namely, blow holes, pipes, and porosities. The chemical composition of each alloy is given in Table 1.

For microstructural investigation, samples of each alloy were sectioned from the Y-blocks and then prepared using standard metallographic techniques (etched with 2% nital). Metallographic samples were examined in an optical microscope. For determining the nodule count, methods suggested by Loper et al. (Ref 7) was used. All big and small nodules visible at a magnification of 200× were considered for counting. However, nodules smaller than 1 mm diameter were neglected. An image processing unit of Leica was used for quantitative determination of percent pearlite and ferrite in the microstructure. For nodule counting, 30 metallographic fields were

scanned. The data reported are average of those 30 readings. For quantitative metallography, 10 to 15 fields have been scanned and the image analysis data have been averaged. Some of the cast samples were also examined in SEM and XRD (Philips Xpert pro) to identify phases more clearly. The distribution of manganese, silicon, and carbon between graphite nodules in the cast alloys was determined with the help of an electron probe micro-analyzer (EPMA). In addition, the distribution of Mn, Si, and Cu in the cast alloys was also mapped in a FE-SEM (Zeiss Make).

Hardness values were measured in a Vickers hardness tester using 20 kg load. Micro-hardness values of the specific phases were determined in a MXT-70 micro-hardness tester (Tokyo, Japan) using 10 g load for ferrite regions and 25 g load for pearlite areas. Test pieces for tension and impact tests were prepared from the coupons of Y-blocks. Tension tests were carried out using an Instron (model 8516) testing machine at a crosshead speed of 1 mm/min and full-scale load of 100 kN. From the load-elongation charts, ultimate tensile strength (UTS) and total elongation values were calculated. Due to shortage of material, only two tensile samples of each alloy could be tested. The UTS and % elongation results represent average of two close readings. The fracture surfaces of as-cast tensile test specimens were examined in a scanning electron microscope (Model: S3000N, Hitachi Ltd, Japan). Impact toughness was measured by a Charpy impact testing machine. Dimension of specimens for tension and Charpy tests is given in Fig. 2, 3.

To determine the critical temperature ranges of alloys A, B, C and D, and also to determine the effect of copper and manganese on critical temperatures, samples of standard dimensions (shown in Fig. 4) were subjected to heating and cooling cycles at a very slow rate. The resultant dilation (dimensional changes) due to contraction and expansion of the samples was measured with the help of a dial gauge. The critical temperatures indicating start and end of austenitization were determined separately for the heating and cooling cycles and then averaged out for the purpose of subsequent heat treatment.

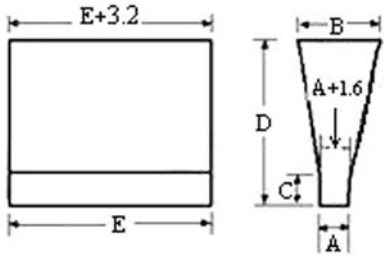

Fig. 1 Y-Block (A = 25.4, B = 55.0, C = 38.1, D = 130.2, and E = 152.4). All dimensions are in mm

3. Results and Discussion

3.1 Casting Quality and Chemical Composition

Table 1 lists the chemical composition of the experimental alloys A, B, C, and D and the corresponding carbon equivalent values. An average retained magnesium content of around 0.04% was adequate for good nodularization of graphite. Since manganese improves hardenability, a fairly high level of manganese was added in alloys B, C, and D. In addition, copper was also introduced in alloys C and D. Such alloy chemistry was designed to study the synergistic effect of combined manganese and copper addition on intercellular segregation and structure-property relationship. In the calculation for % CEV, the contribution of C, Si, Mn, Cu, and P is taken into account. The said alloys also contain trace elements, namely, Cr—0.01%, Mo—0.005%, Sn—0.02%, and Ti—0.025-0.03%.

3.2 Microstructures

The light micrographs of the as-cast alloys A, B, C, and D, in both etched and un-etched conditions, are given in Fig. 5 and 6. Microstructures of the unetched samples (Fig. 5a-d) show

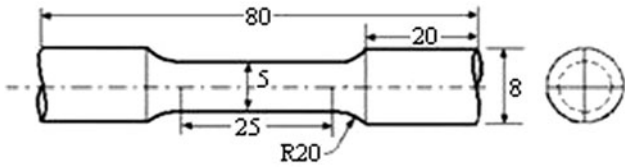

Fig. 2 Tensile test specimen. All dimensions are in mm

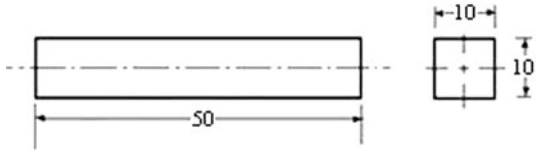

Fig. 3 Impact test specimen. All dimensions are in mm

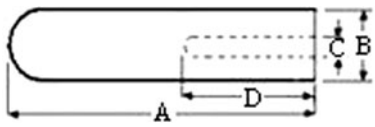

Fig. 4 Dilatometry test specimen (A = 50, B = 10, C = 5, and D = 25). All dimensions are in mm

Table 1 Chemical composition, wt.%

Alloys	C	Si	Mn	S	P	Cu	Mg	CEV(a)
A	3.18	2.64	0.45	0.012	0.016	…	0.038	4.140
B	3.35	2.51	0.82	0.012	0.018	…	0.035	4.380
C	3.16	2.80	1.08	0.011	0.015	0.56	0.042	4.318
D	3.18	3.00	1.04	0.011	0.016	1.13	0.045	4.429

(a) CEV% = %C + %(Si + P)/3 + %Mn/6 + %Cu/13

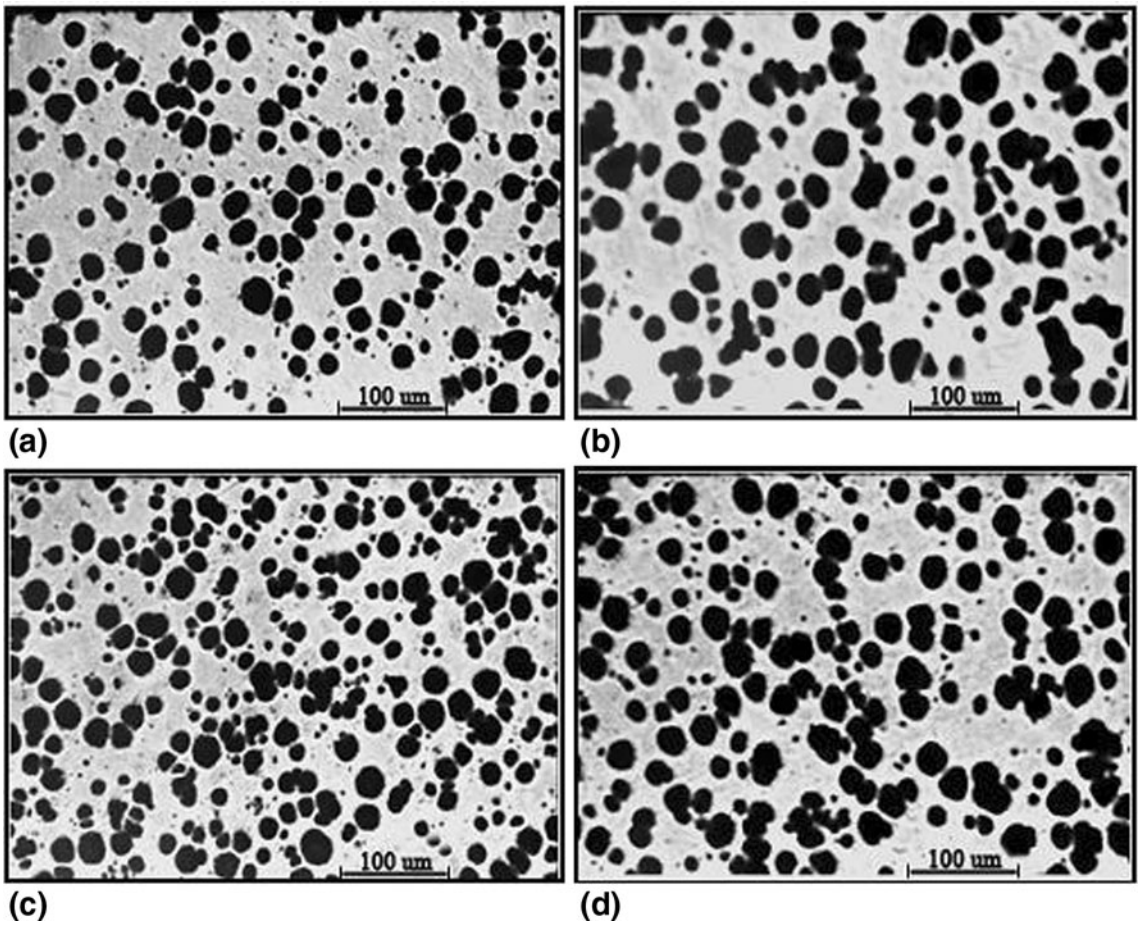

Fig. 5 Optical micrographs of un-etched samples to reveal the size and distribution of graphite nodules: (a) alloy A, (b) alloy B, (c) alloy C, and (d) alloy D

clearly the shape, size, and distribution of graphite nodules. The micrographs of etched samples reveal the relative proportions of ferrite and pearlite (Fig. 6a-d) in those samples. A summary of the quantitative measurements on nodule count, nodularity and the relative proportions of different phases are given in Table 2 and 3, respectively. As illustrated in the micrographs, the microstructures of alloys A, B, and C are predominantly pearlitic with bull's eye ferrite enveloping the graphite nodules. However, alloy D does not show any free ferrite around the graphite nodules. Since, manganese and copper are pearlite stabilizers, the progressive increase of these elements, either singly or in combination, from alloy A to D resulted in an increase in the pearlite content (Table 3).

There was only a marginal change in the nodule count and pearlite content on raising the manganese content from 0.45% in alloy A to 0.82% in alloy B. The carbon equivalent in alloy B was slightly higher than that in A. In alloys C and D, nodule count increased but the proportion of free ferrite decreased appreciably. In fact, there was practically no free ferrite in alloy D, which was alloyed with about 1.0% manganese and 1.0% copper. Both manganese and copper are pearlite stabilizers. Among the common alloying elements, silicon is the strongest graphitizer and it raises the carbon equivalent value appreciably. The nodule count in alloy C increased mainly because of its higher silicon content and increased carbon equivalent value. A further increase in copper content in alloy D from 0.5 to 1.0% resulted in a drop in nodule count. The silicon content in alloy D is higher than that in alloy C, while the carbon equivalent is nearly equal to that of alloy C. The effect of interaction of copper with other alloying elements on nodule count needs to be investigated further in future. Copper is reported to be an effective strengthening element, and its pearlite promoting role is appreciated only when it is combined with at least a low addition of manganese (Ref 4, 5). The results of the present investigation confirm this.

3.3 Mechanical Properties

The data obtained from hardness, tensile, and impact tests on the as-cast alloys are reported in Table 4. The mechanical property changes are more or less consistent with variations in composition and microstructure. The gradual hardening of the matrix with increasing addition of manganese and copper is also on the line of expectation (Ref 4, 5). It is apparent from Table 4 that the present series of alloys possess relatively low as-cast impact strength and only a moderate UTS and ductility. The results, however, satisfy the requirements of the targeted BS 600/3 and 700/2 grades of ductile irons and broadly match those of Japanese workers (Ref 8).

Among the experimental alloys, alloy A possessed reasonably good strength and ductility. But the superior UTS (813 MPa) and lower ductility (5.0%) in alloy D is obviously due to high dose of alloying with Cu + Mn and consequent changes in microstructure. Alloy C with a slightly lower

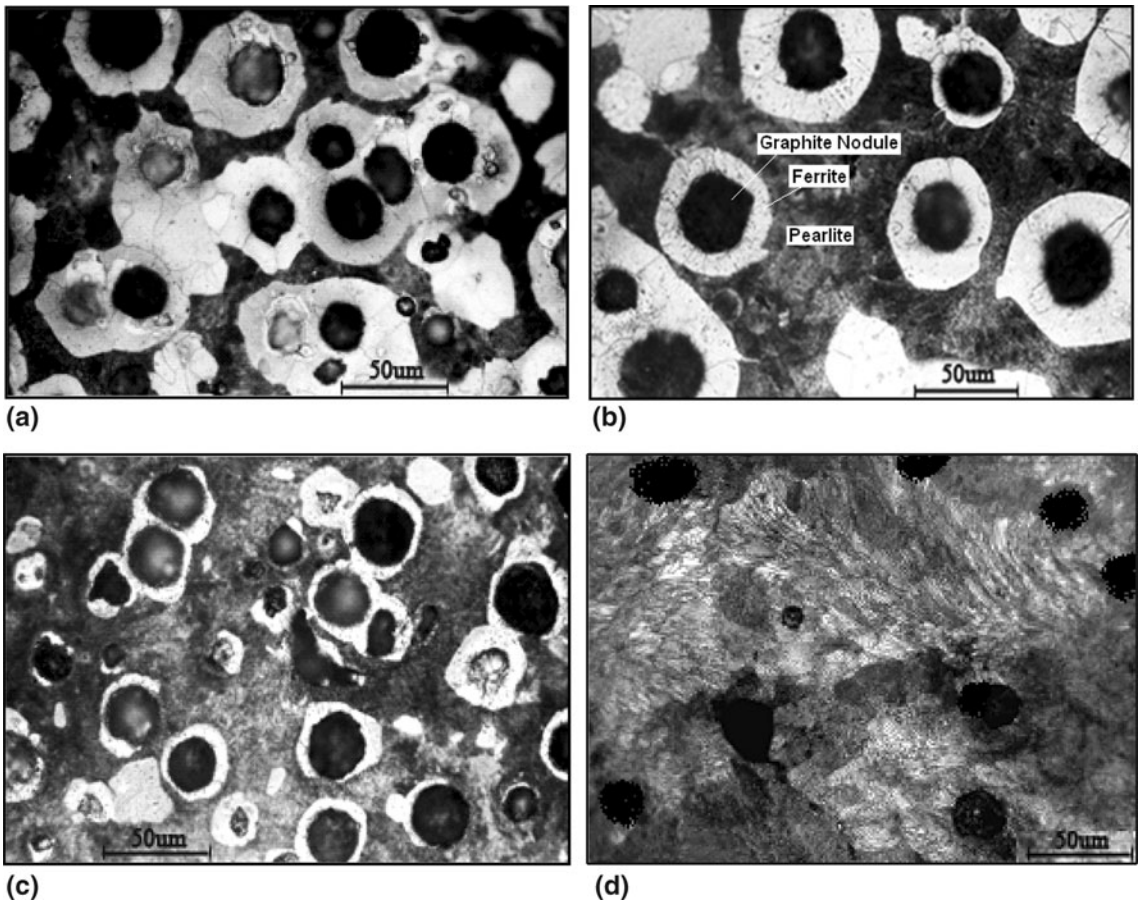

Fig. 6 Optical micrographs of etched samples showing different proportions of ferrite and pearlite: (a) alloy A, (b) alloy B, (c) alloy C, and (d) alloy D

Table 2 Graphite statistics

Alloys	Volume% graphite	Nodule count number, mm^2	Nodularity
A	14	115	>85
B	16	110	>85
C	16	180	>85
D	20	130	>85

Table 3 Approximate volume percent of phases in the matrix (excluding the graphite content)

Alloys	Volume % of ferrite	Volume % of pearlite
A	20	66
B	20	64
C	10	74
D	Trace	80

pearlite content developed a relatively better combination of UTS of 750 MPa and elongation >6%. In fact, the micro-hardness values of the ferrite phase have been found to be significantly higher in alloy C as compared to that in alloys A and B (Table 5), which also contributed to its strengthening.

Table 4 Mechanical properties

Alloy	Hardness, HV	UTS, MPa	% Elongation	Charpy impact strength, J
A	205	800.00	8.6	7.85
B	220	600.00	8.0	7.0
C	275	753.00	6.4	5.9
D	283	813.00	5.3	4.0

In contrast to the above, Charpy impact test results (Table 4) indicate that the toughness of the experimental alloys was generally low. The base alloy A developed a marginally higher impact toughness of nearly 8 J, perhaps due to suitable combinations of ferrite, pearlite, and nodule count. In the remaining alloys B, C and particularly in alloy D, the toughness goes down as more and more pearlite replaces the ductile ferrite phase (Table 3). Although these alloys fulfilled the strength-ductility requirement of 700/2 and 600/3 grades of ductile iron, their low toughness appears to be a matter of concern. So, the samples were examined in a scanning electron microscope. In SEM examination, the existence of martensite patches in association with pearlite colonies was revealed in all the alloys. Typical SEM photographs of the as-cast samples presented in Fig. 7 illustrate these microstructural features. Increasing manganese alone or in combination with copper raised the

hardenability of the cast alloys to an extent that some martensite also formed during transformation of austenite below critical temperature. The relatively high micro-hardness of the pearlitic areas (Table 5) also suggests the presence of a hard martensite phase, which contributed to reduction of impact toughness of the as-cast alloys. Further, the volume fraction of martensite in alloys A and B was relatively low and it was more in Cu + Mn alloyed irons C and D. Naturally, the toughness also deteriorated in the same order.

XRD was also carried out to locate the microstructural features responsible for such poor performance under impact loading. As shown in Fig. 8, the XRD patterns of alloys A, B, C, and D reveal the presence of martensite in the as-cast alloys. The presence of clear doublets in the XRD patterns is due to the formation of martensite, as indentified by Cullity (Ref 9). However, the microstructure analysis reported above presents the prospect of improving the toughness of cast alloys through tempering. The selection of the tempering temperature will depend up on the exact requirement of strength-ductility-toughness combination.

Table 5 Micro-hardness values

	Hardness, HV	
Alloy	**Ferrite**	**Pearlite**
A	180	370
B	203	390
C	224	390
D	…	428

3.4 Fractography and Electron Microprobe Analysis

The fracture patterns in the present series of alloy samples match those of ferrito-pearlitic and pearlitic samples reported earlier (Ref 10-14). The fractures are primarily transgranular with some evidence of inter-granular cracking as well. In alloys A, B, and C, there is also evidence of micro-void coalescence around nodules (Fig. 9a-c). The fractograph of alloy D, on the contrary, shows only transgranular and intergranular cleavage facets (Fig. 9d). The nodules were also sheared in most cases in this alloy.

Figures 10 and 11 show the results of microprobe analysis of manganese, silicon, and copper distribution in as-cast alloys C and D, containing relatively larger contents of alloying elements. These distribution maps show some silicon segregation near the graphite nodules and little segregation of manganese. It is very likely that moderate nodule counts in alloys C and D favoured reduction of manganese segregation at the cell boundaries. In addition, the riser portion of a Y-block

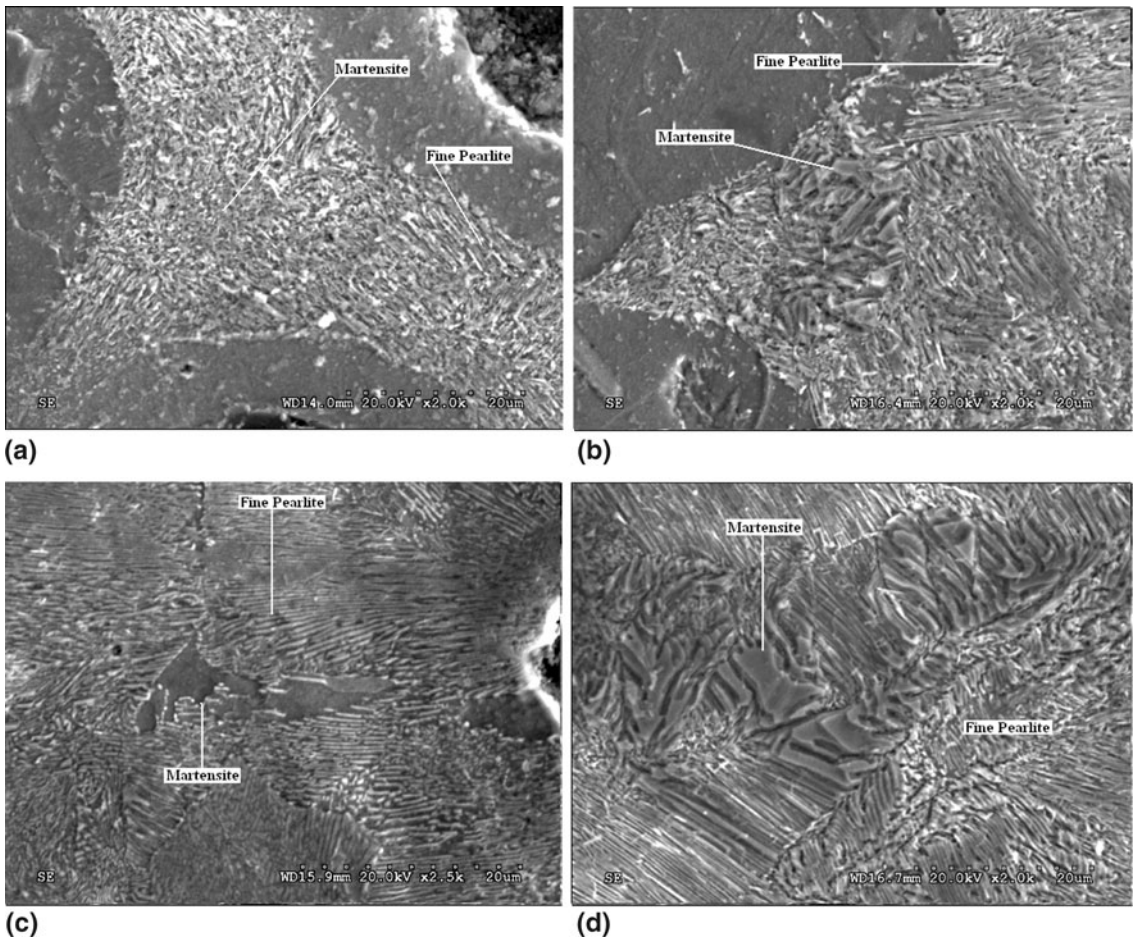

Fig. 7 SEM micrographs of as-cast alloys A, B, C, and D (martensite areas are marked by arrows)

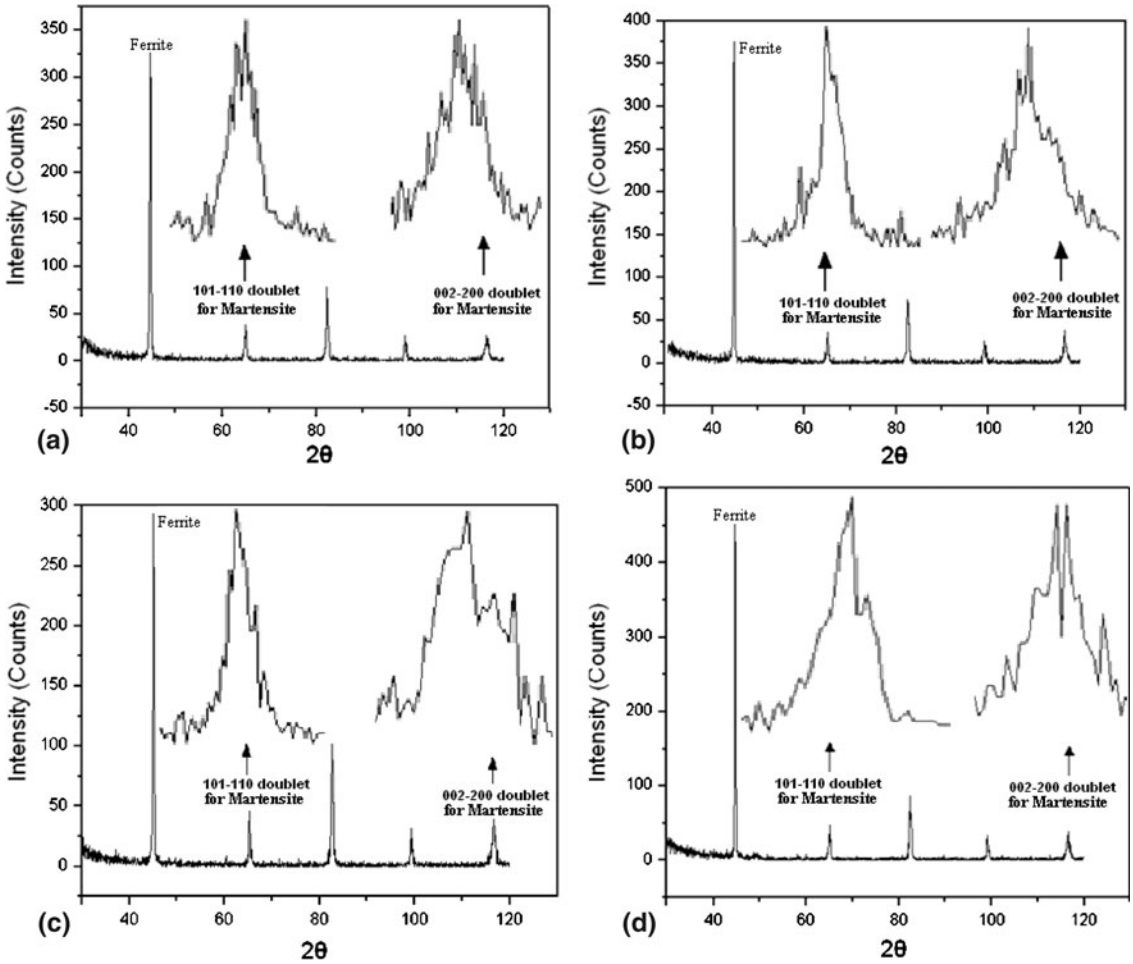

Fig. 8 X-ray diffraction patterns of as-cast Alloys A, B, C, and D. Peaks marked by arrow are blown-up to show martensite doublet

cools at a slower rate than the 25 mm section thickness coupon from which the present as cast samples are drawn. Possibly due to heat flow from the riser portion, the coupon also cools at a slow rate leading to minimization of micro-segregation. Further, elemental mapping is carried out on alloys C and D and the corresponding maps shown in Fig. 12(a) to (d) do not indicate the presence of any manganese segregation. Manganese-rich carbide which is normally present in manganese segregated zones (Ref 15) could not be detected in any of the SEM secondary electron images. This is also an indication of absence of manganese segregation.

Ahamadabadi et al. (Ref 16) made a similar study on segregation of manganese and silicon in a 1% manganese ductile iron. Their work suggests that a shorter solidification time enhances inoculation efficiency and increases nodule count with a consequent reduction of segregation of alloying elements (Mn and Si) in the intercellular regions. 25 mm thick Y-block castings are not thin section castings; hence any influence of fast cooling is ruled out in the present case. Since, both manganese and copper are FCC metals and are austenite stabilizers, it is suspected that the solubility of manganese in austenite dendrites in a solidifying casting is appreciably increased when Cu + Mn are added together. This phenomenon further assists in reducing the tendency of manganese to segregate at the eutectic cell boundary.

3.5 Critical Temperatures

To recover the strength and toughness of ductile irons, suggested heat treatment practices are quenching and tempering or isothermal transformation treatments involving austenitisation as a primary step. The knowledge of critical temperatures is certainly important to optimize the austenitising temperature of any alloy. Therefore, the critical temperatures of the experimental ductile irons were measured and the values are given in Table 6. An average of A_s (austenite start temperature) and P_f (pearlite finish temperature) was determined to find out the lower critical temperature; while the A_f (austenite finish temperature) and P_s (pearlite start temperature) were averaged to find out the upper critical temperature.

Silicon and manganese contents in an iron-carbon system influence the critical temperature range in opposite manner. While silicon is known to raise the critical temperatures, manganese depresses the same (Ref 17). Copper also raises the critical temperatures, but its effect is not as strong as that of silicon. The combined influence of these alloying elements on the critical temperatures of the experimental alloys may be appreciated from the data presented in Table 6. Austenite formation temperature on heating dropped in alloy B on raising the manganese content from 0.45 to 0.82%. But, on simultaneous addition of copper and manganese it increased again.

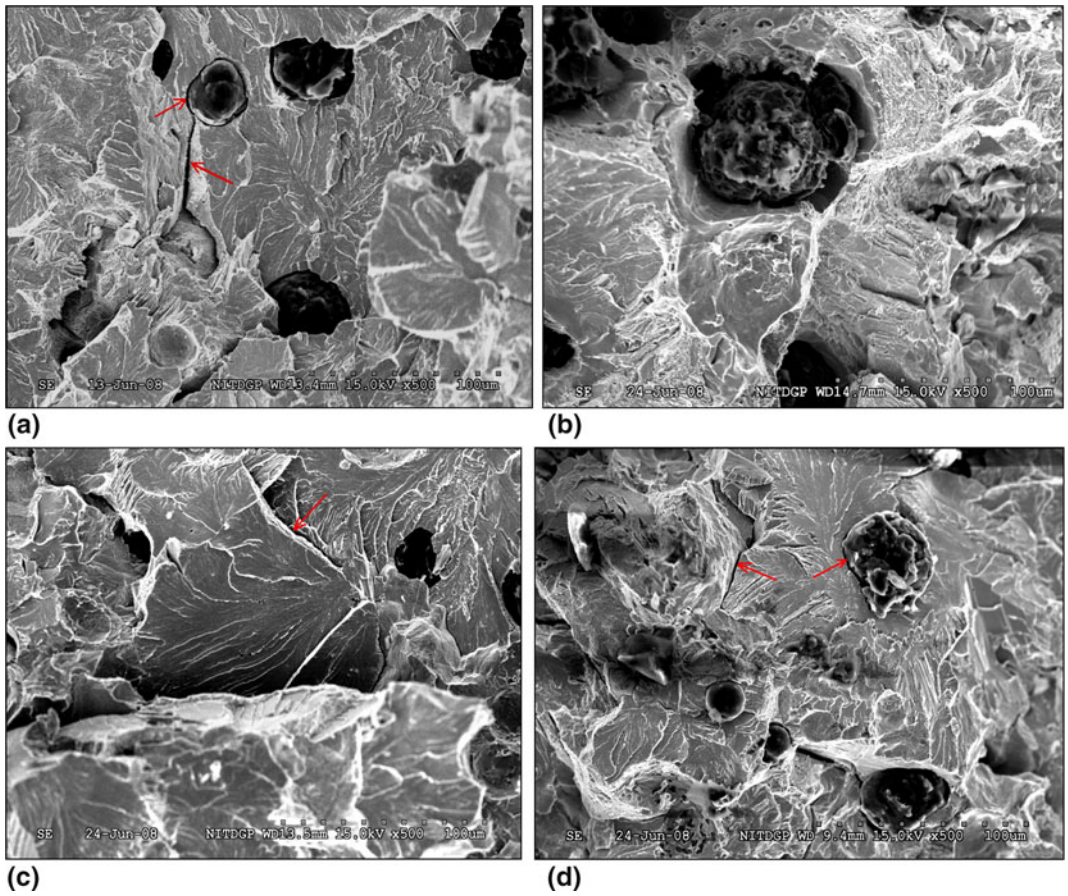

Fig. 9 SEM fractographs of alloys A, B, C, and D after tensile testing

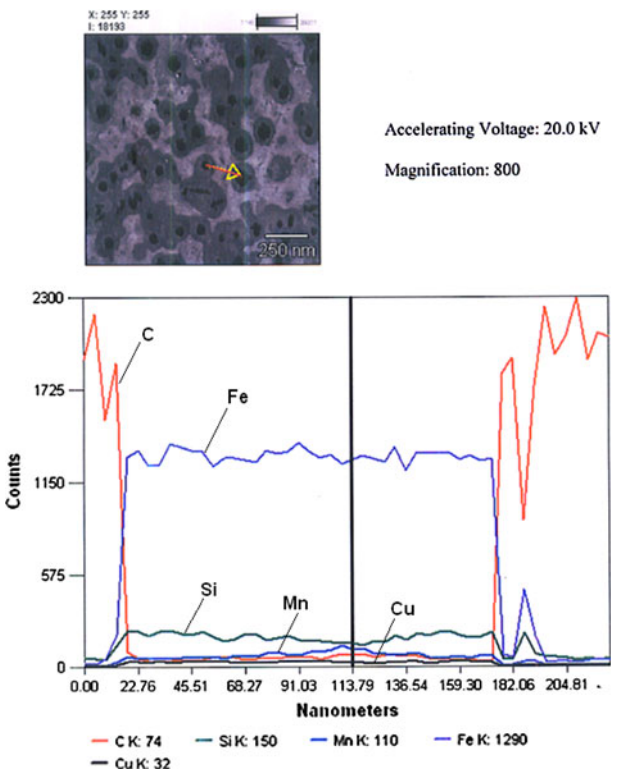

Fig. 10 Results of microprobe analysis of alloy C for measurement of Mn, Si, C, and Cu segregation

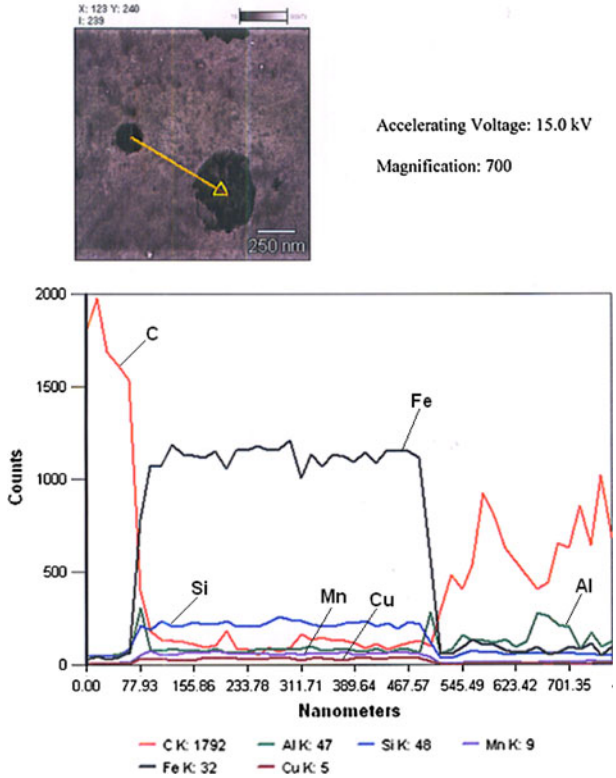

Fig. 11 Results of microprobe analysis of alloy D for measurement of Mn, Si, C, and Cu segregation

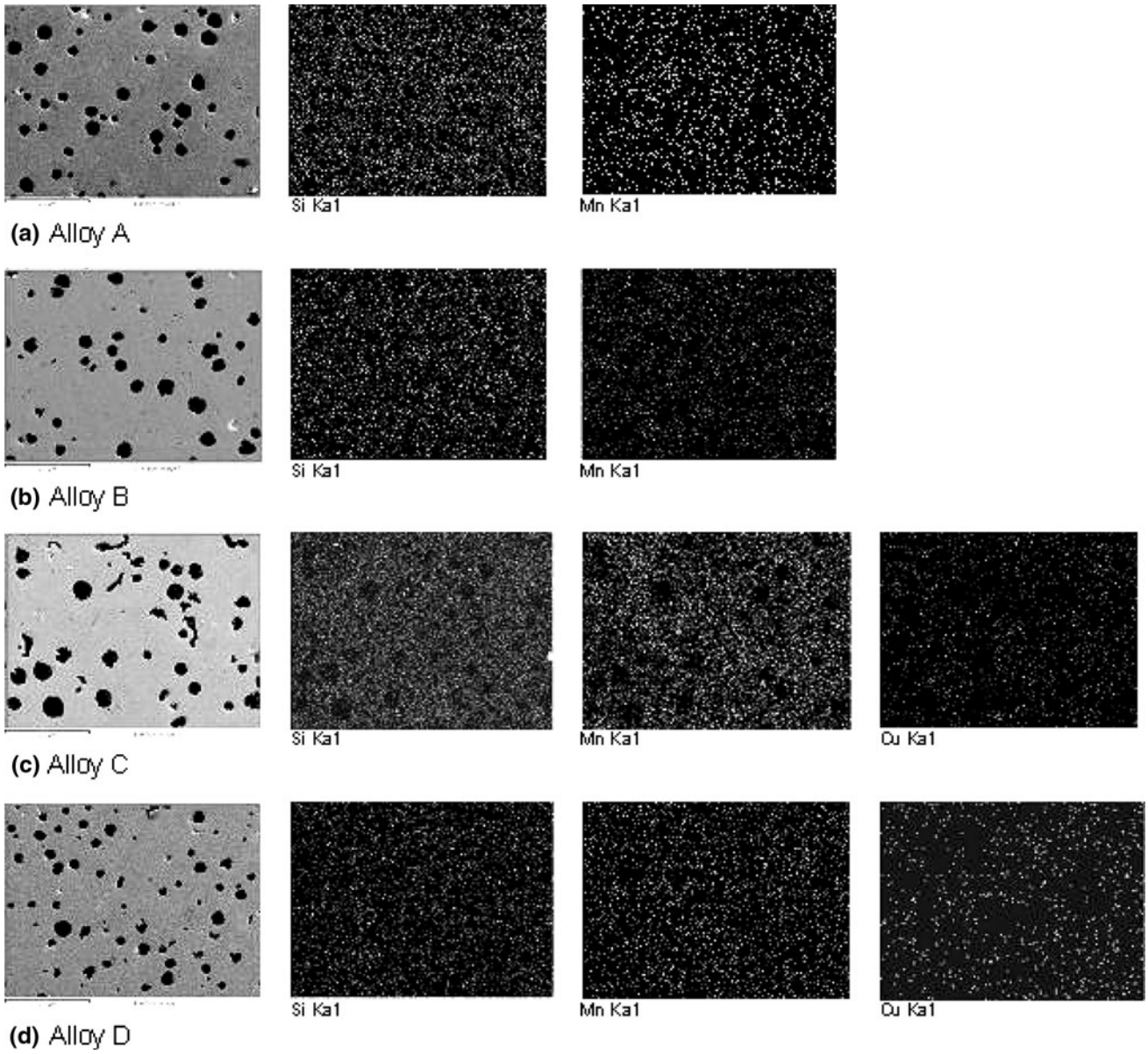

Fig. 12 Dot maps showing distribution of elements in alloys A to D

Table 6 Critical temperature ranges

Alloys	A_s, °C	A_f, °C	P_s, °C	P_f, °C	Critical temp. range, °C
A	800	860	775	730	765-817
B	750	830	760	690	720-795
C	780	820	725	700	740-772
D	775	825	755	730	752-790

Similar changes in pearlite formation temperature occurred during cooling. The critical temperatures in the four experimental alloys were found to vary between a minimum and a maximum, as shown in the Table 6. Based on these data, it would be easier to try out suitable austenitization temperatures for subsequent heat treatment processes of the said ductile irons.

4. Conclusion

(1) The progressive increase of manganese and copper, either singly or in combination, from alloy A to D resulted in an increase in pearlite content. There was, practically, no free ferrite in alloy D.
(2) There was a gradual hardening of the alloys with increasing addition of manganese and copper. The alloys exhibited relatively low impact strength and moderately good UTS and ductility.
(3) Relatively high pearlite hardness and presence of hard martensite phase in the matrix microstructure contributed to reduction in impact toughness in the experimental alloys.
(4) SEM fractographs of the as-cast alloys show predominantly transgranular cleavage fracture mode.
(5) Microprobe analysis shows some silicon segregation near the graphite nodules, but little segregation of manganese.

Elemental mapping by FE-SEM do not indicate any manganese segregation.

(6) Critical temperature, namely, the austenite start temperature on heating dropped by raising the manganese content from 0.45% in alloy A to 0.82% in alloy B. But on simultaneous Cu + Mn addition in alloys C and D, it increased again.

Acknowledgment

Financial support by National Institute of Technology, Durgapur, India is gratefully acknowledged.

References

1. R. Elliott, *Cast Iron Technology*, Butterworth & Co (P) Ltd, London, 1988, p 107
2. E. Dorazil, B. Batra, E. Munsterova, L. Stransky, and A. Huvar, High Strength Bainitic Ductile Cast iron, *A. F. S Int. Cast Met. J.*, 1982, **52**, p 7
3. S. Christophe and J. Lacarze, Study of Microsegregation Building up During Solidification of Spheroidal Graphite Cast Iron, *Met. Mater. Trans. B*, 2000, **31B**, p 827–836
4. J. Lacarze, Solidification of Spheroidal Graphite Cast Irons: III. Microsegregation Related Effects, *Acta Mater.*, 1999, **47**(14), p 3779–3792
5. M.M. Shea, Influence of Cooling Rate and Mn and Cu Content on Hardness of As Cast Ductile Iron, *A.F.S. Trans.*, 1978, **86**, p 7–12
6. J. Lacarze, The Role of Mn and Cu in the Eutectic Transformation of Spheroidal Graphite Cast Iron, *Met. Mater. Trans A*, 1997, **28**(10), p 2015–2025
7. C.R. Loper, P.S. Nagarseth, and R.W. Heine, Nodule Count and Ductile Iron Quality, *Gray Iron News*, June (1964) 5
8. H. Takumi, K. Toshinori, Y. Tooru, and H. Sadato, Effect of Graphite Nodule Count and Pearlite Lamellar Spacing on Mechanical Properties of Fine Pearlite S.G. Iron, *J. Jpn. Foundry Eng. Soc.*, 2004, **76**(11), p 891–896
9. B.D. Cullity, *Elements of X ray Diffraction*, 2nd ed., Addison-Wesley Publishing Co. Inc., Reading, 1978, p 412–413
10. A.S. Lazaridis, F.J. Worzala, C.R. Loper, and R.W. Heine, Fracture Toughness of Ductile Cast Iron, *A. F. S. Trans.*, 1971, **79**, p 351–360
11. R.K. Nanstad, F.J. Worzala, and C.R. Loper, Jr., Static and Dynamic Toughness of Ductile Cast Iron, *A. F. S. Trans.*, 1975, **83**, p 245
12. J.O.T. Adeware and C.R. Loper, Jr., Effect of Pearlite on Crack Initiation and Propagation in Ductile Iron, *A. F. S. Trans.*, 1976, **84**, p 513–526
13. J.O.T. Adeware and C.R. Loper, Jr., Crack Initiation and Propagation in Fully Ferritic Ductile Iron, *A. F. S. Trans.*, 1976, **84**, p 527–534
14. R.K. Nanstad, F.J. Worzala, and C.R. Loper, Jr., Fracture Toughness Testing of Nodular Cast Iron, *A. F. S. Trans.*, 1974, **89**, p 473–486
15. E.C. Muratore, *Sorelmetal Suggestions for Ductile Iron Production, Case study No. 107*, Rio Tinto Iron & Titanium Inc., Montréal, Canada, 2006
16. M.N. Ahamdabadi, E. Niyama, and T. Ohide, Structural Control of 1.0% Mn ADI, Aided Modeling of Micro Segregation, *A. F. S. Trans.*, 1994, **120**, p 269–278
17. A.T. Angus, *Cast Iron—Physical and Engineering Properties*, Butterworth and Co. (P) Ltd., London, 1976, p 12–15